Spacecraft Attitude Determination with Sun Sensors, Horizon Sensors and Gyros: Comparison of Steady-State Kalman Filter and Extended Kalman Filter

Vaibhav V. Unhelkar and Hari B. Hablani

Indian Institute of Technology Bombay, Powai, Mumbai, India
v.unhelkar@iitb.ac.in, hbhablani@aero.iitb.ac.in

Abstract. Attitude determination, along with attitude control, is critical to functioning of every space mission. In this paper, we investigate and compare, through simulation, the application of two autonomous sequential attitude estimation algorithms, adopted from the literature, for attitude determination using attitude sensors (sun sensor and horizon sensors) and rate-integrating gyros. The two algorithms are: the direction cosine matrix (DCM) based steady-state Kalman Filter, and the classic quaternion-based Extended Kalman Filter. To make the analysis realistic, as well as to improve the attitude determination accuracies, detailed sensor measurement models are developed. Modifications in the attitude determination algorithms for estimation of additional states to account for sensor biases and misalignments are presented. A modular six degree-of-freedom closed-loop simulation, developed in house, is used to observe and compare the performances of the attitude determination algorithms.

Keywords: Attitude Determination, Kalman Filter, Horizon Sensors.

1 Introduction

Maintaining a desired orientation in space, with a specified level of accuracy, is a mission requirement for every spacecraft. Attitude determination along with attitude control is responsible for satisfying this requirement. Based on the function of the spacecraft the level of pointing accuracy required varies. During the past four decades, extensive research has been done in the area of spacecraft attitude determination. Various algorithms exist in the literature, with varied level of complexity and applicability [1]. The choice of algorithm for a mission depends on pointing accuracy requirements, the type of sensors available and capability of the on-board computer.

Here, we consider analysis of the attitude determination subsystem for Low Earth Orbit satellites using sun sensors, horizon sensors and fiber optic gyros to achieve three-axis pointing accuracy requirement of 0.1 deg. To make the analysis of these algorithms realistic, as well as to improve the accuracy of the

D. Choukroun et al. (eds.), *Advances in Estimation, Navigation, and Spacecraft Control*,
DOI: 10.1007/978-3-662-44785-7_22

attitude determination algorithms, detailed models of measurements with sun sensor, horizon sensor and gyros are utilized. Instead of treating measurement errors as white noise, an effort is made to develop realistic systemic errors and noise models. For instance, horizon sensor modeling includes errors arising from Earth's oblateness, atmospheric radiance and sensor electronics.

Further, a modular six degree-of-freedom closed-loop MATLAB-Simulink® simulation is developed, which comprises true attitude kinematics and dynamics, sensor models, orbit propagation, attitude determination and control. This simulation setup is used to compare the performances of the attitude determination algorithms developed. The modular design of simulation allows a straight forward approach to include or exclude sensors and to test different attitude estimators and controllers.

Two attitude estimation algorithms are considered, which mainly vary with respect to their attitude representations and computational requirements. First, a steady-state Kalman Filter, adopted from [2], is analyzed and simulated to obtain estimates of satellite attitude and gyro drift rate bias. Direction cosine matrix and Euler angles are used to represent the attitude, for ease of physical interpretation. The steady-state formulation does away with expensive matrix covariance computations, but if dictated by mission requirements the formulation can be easily modified to its recursive gain counterpart. This is followed up with the analysis and simulation of the classic quaternion-based Extended Kalman Filter of Lefferts, Markley and Shuster [3] for the on-board sensor suite considered . The classic EKF is modified to estimate exponentially-correlated radiance error in horizon sensor measurements. Lastly, the effect of sensor misalignments on attitude estimation performance is assessed through simulations, and Pittelkau's remedy to mitigate the performance degradation due to the misalignments, i.e., alignment Kalman filter [4], is presented.

Reference Frames

We consider three frames of reference. The Earth-centered Inertial (ECI) frame is an inertial frame with origin at the Earth's center. The coordinate axes $\mathbf{x}_I$ and $\mathbf{z}_I$ point towards the direction of the vernal equinox and the north pole, respectively, and $\mathbf{y}_I$ completes the right-handed coordinate system. The Local Vertical Local Horizontal (LVLH) frame describes the current orbit frame of the satellite, and has its origin at the center of mass of the satellite. The coordinate axis $\mathbf{z}_L$ points towards the center of the earth (direction of the nadir), $\mathbf{y}_L$ points opposite to the satellite's angular momentum, and $\mathbf{x}_L$ completes the right-handed triad. The instantaneous LVLH frame is used as reference to measure the local attitude of the satellite. Body frame is an orthogonal coordinate system fixed to the satellite body with origin at its center of mass.

The symbols $\hat{\mathbf{x}}$ and $\mathbf{x}^{\times}$ denote the estimate and the cross-product matrix associated with $\mathbf{x}$, respectively.

2 Sensor Models

This section briefly describes the sensor models for the sensor suite considered. As these sensors have been used in various space missions, sufficient technical research exists regarding their characteristics and performance [5,6]. However, in spite of the literature, usually additional analysis is required to arrive at customized and realistic model of these sensors (especially so for the attitude sensors) based on the sensor configuration of a particular spacecraft.

2.1 Rate-Integrating Gyros

Gyros are inertial sensors which measure change in attitude as opposed to the absolute attitude. Gyros are of various types, such as, mechanical gyros, ring laser gyros, fiber optic gyros, and can be classified based on their accuracy, mechanisms and form of output. Rate gyros measure angular rate directly, while the rate-integrating gyros (RIG) measure integrated angular rate [1]. In our attitude determination study, we consider application of fiber optic rate-integrating gyros, which provide incremental angle vector.

The measurement equation which, essentially, corresponds to the inertial rate of the body expressed in body frame $\boldsymbol{\omega}_{BI}^{B}$ corrupted by various noise sources is given as,

$$\boldsymbol{\omega}_m = \mathrm{A}_{malgn}\boldsymbol{\omega}_{BI}^{B} + \mathbf{b} + \boldsymbol{\eta}_g \tag{1}$$

$$\dot{\mathbf{b}} = \boldsymbol{\eta}_u \tag{2}$$

where, the subscript 'm' denotes the measured rate, $\mathbf{b}$ denotes the gyro drift-rate bias, A_{malgn} denotes the misalignment and scale factor matrix matrix, and $\boldsymbol{\eta}_g$ (random-walk rate vector) and $\boldsymbol{\eta}_u$ (drift acceleration) are two continuous time white noise vectors. These equations when converted to discrete time yield [7],

$$\Delta\boldsymbol{\varphi} = \Delta\boldsymbol{\theta} + T_{gyro}\mathbf{b}_k + \boldsymbol{\beta}_k + \boldsymbol{\nu}_{q,k} \tag{3}$$

$$\text{where} \quad \boldsymbol{\omega}_{in} = \mathrm{A}_{malgn}\boldsymbol{\omega}_{BI}^{B} \tag{4}$$

$$\Delta\boldsymbol{\theta} = \int_{kT_{gyro}}^{(k+1)T_{gyro}} \boldsymbol{\omega}_{in}(t)dt \tag{5}$$

The term $\Delta\boldsymbol{\theta}$ expresses the true change in the spacecraft attitude, whereas the $\Delta\boldsymbol{\varphi}$ denotes the rate-integrating gyro output during one gyro sample period (T_{gyro}). The zero-mean noise due to $\boldsymbol{\eta}_g(t)$ and $\boldsymbol{\eta}_u(t)$ is expressed by $\boldsymbol{\beta}_k$. The variance of $\boldsymbol{\beta}_k$ is a 3×3 diagonal matrix for which the diagonal element is $\sigma_\beta^2 = \sigma_v^2 T_{gyro} + \sigma_u^2 T_{gyro}^3/3$, where σ_v^2 (rad^2/s) and σ_u^2 (rad^2/s^3) are power spectral densities of the scalar elements of $\boldsymbol{\eta}_g$ and $\boldsymbol{\eta}_u$, respectively. The gyro drift-rate bias evolves in discrete-time as,

$$\mathbf{b}_k = \mathbf{b}_{k-1} + \boldsymbol{\alpha}_k \tag{6}$$

where, $\boldsymbol{\alpha}_k$ is a zero-mean discrete random-rate noise vector, with variance of each element being $\sigma_\alpha^2 = \sigma_u^2 T_{gyro}$ [2]. The term $\boldsymbol{\nu}_{q,k}$, a discrete-time white noise with

variance σ_e^2, represents the quantization error of the gyro. Lastly, scale factor and misalignment errors occur due to mounting errors of the system, or due to intrinsic sensor errors. We use the notation of Pittelkau [4] to define the scale factor and misalignment matrix, where λ_j denotes the scale factor error, while δ_{ij} denotes the axis misalignment,

$$\mathrm{A}_{malign} = \begin{bmatrix} (1+\lambda_x) & -\delta_{yz} & \delta_{zy} \\ \delta_{xz} & (1+\lambda_y) & -\delta_{zx} \\ -\delta_{xy} & \delta_{yx} & (1+\lambda_z) \end{bmatrix} \tag{7}$$

For simulations presented later, we have used parameters of a fiber optic gyro (Table 1). Initial value of gyro drift rate bias is taken as 0.05 deg/hr.

Table 1. Gyro Parameters

Parameter	Value	Units
σ_v	7.27	μrad/s$^{1/2}$
σ_u	3×10^{-4}	μrad/s$^{3/2}$
σ_e	15	μrad

2.2 Sun Sensors

Sun sensors measure the direction of the sun relative to the spacecraft, and provide an attitude reference. These sensors measure the impinging solar energy on their surface and determine the angle made by the sun with respect to the sensor, which in turn is used to arrive at the sun vector. The sun vector, along with a sun model, can also be used to determine the yaw attitude of the spacecraft. However, as the sun sensors measure the radiation from the sun they can function only in the sun-lit phase of the orbit.

The model of sun sensor being used for a particular satellite depends on the type of the sensor, its positioning and error characteristics. For our analysis, we assume six solar cells (represented by blue circles in Fig. 1) placed on each side of the satellite. This configuration and the sun vector construction algorithm is adapted from that of the Pratham student-satellite [8], and has the advantage

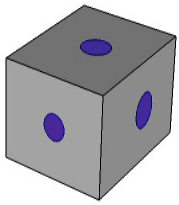

Fig. 1. Sun Sensor Configuration

that in the sun-lit phase the sun is usually visible to three of the sun sensors. Each of the individual cell measures, with some noise, the cosine of the angle made between the Sun vector ($\mathbf{s}$) and the solar cell vector ($\mathbf{c_i}$). The measurement model for one individual solar cell is given by

$$u_i = \mathbf{c_i}_B \cdot \mathbf{s}_B + \nu_c, \forall i = 1:6 \tag{8}$$

The noise in the measurement arises due to the sensor mechanism, electronics, and quantization, the strength of which depends on the type of the sensor. Lastly, each of the cell has a limited field-of-view, hence the measurement model equation (Eq. 8) is valid only within the FOV of each sensor. The sensor parameters for simulation have been taken corresponding to that of a single-axis solar cell [6], as listed in Table 2.

Table 2. Sun Sensor Parameters

Parameter	Value	Units	Remark
σ_c	0.05	deg	Standard Deviation of ν_c
FOV	80	deg	Field-of-View (conical)
T_c	1	s	Sample Time

These measurements are then used to determine the Sun vector through elementary linear transformation [8], which is then used in the attitude determination formulations. The measured Sun vector can be represented as,

$$\mathbf{s}_{m,B} = \mathbf{s}_B + \tilde{\mathbf{s}}_{m,B} \tag{9}$$

where, $\tilde{\mathbf{s}}_{m,B}$ is a random zero-mean Gaussian variable, with noise covariance, $\mathrm{R}_c = \sigma_c^2 \mathbf{I}_{3\times 3}$.

2.3 Horizon Sensors

Horizon sensors, essentially, measure the direction of Earth (nadir) by observing the shape of the Earth's limb as seen from the spacecraft and comparing it with a modeled shape, to arrive at the spacecraft attitude. These can be classified into two types - scanning and static - which differ in their mechanism to sense the Earth's horizon, error characteristics and field-of-view. The horizon sensors measure roll and pitch angles. Thus, in the sun-lit phase, along with the sun sensor the horizon sensor provide complete attitude information. We consider scanning-type horizon sensors, and follow the work presented in [9,10,11] for their analysis and error characteristics.

Scanning type horizon sensors consist of moving optical scanners mounted on the spacecraft, which scan and detect the Earth's limb. The sensor electronics converts the radiation information to scan width of Earth's limb. This measurements of scan width are then processed to obtain measurements of roll and pitch. The scanning type sensors though relatively less accurate have a much larger field-of-view than the static horizon sensors.

Mathematical Model. The horizon sensor configuration considered involves two optical scanners mounted on opposite sides of the spacecraft in the pitch-yaw plane. These two scanners measure four semi-scan angles - ($\theta_{\omega 0R}$,$\theta_{\omega 1R}$,$\theta_{\omega 0L}$, and $\theta_{\omega 1L}$) - corresponding to the space-to-earth and earth-to-space transition of left and right scanners. For a detailed description of the sensor configuration the reader is directed to [11]. In order to generate the scan width measurements based on the semi-scan angles due to an oblate earth model, we use the equations specified in [11] and [12], along with the model of oblate earth by Liu [5], with appropriate modifications to suit our coordinate convention. Once the four semi-scan angles are obtained, the roll and pitch angles are obtained as follows [11],

$$\phi = \frac{1}{4} K \left(\theta_{\omega 0R} + \theta_{\omega 1R} - \theta_{\omega 0L} - \theta_{\omega 1L}\right) \tag{10}$$

$$\theta = \frac{1}{4} \cos\xi \left(\theta_{\omega 0R} - \theta_{\omega 1R} + \theta_{\omega 0L} - \theta_{\omega 1L}\right) \tag{11}$$

where, K and ξ are known parameters which depend on spacecraft's altitude and sensor hardware parameters.

The horizon sensor measurements are affected both by the noises in electronics and the errors arising from the limitation in accurately modeling the Earth's limb. The major sources of horizon sensor errors are Earth's oblateness, variation of Earth's radiation, electronic noise, quantization error, and sensor bias and misalignment [9]. Errors due to Earth's oblateness are systemic and highly predictable. Thus, by using an appropriate model of Earth's shape these errors can be largely eliminated. We follow the approach described in [11] to account for errors due to oblateness. Earth's radiation suffers from seasonal and latitudinal variations, which are partly systemic and partly stochastic [13]. The systemic variations can be largely corrected based on modeling of sensor optics and Earth's radiation. The available horizon sensor hardware largely compensates for these systemic variations internally; however, stochastic errors of the order of 0.06 deg still persist post corrections [9]. Sensor bias, misalignment and electronic noise are inherent sensor errors that arise due to the sensor hardware.

For simulation, the roll and pitch angles obtained from Eq. (10-11) are corrupted with bias, white noise (to simulate the electronic noise) and noise due to

radiance. Radiance models exist in literature based on analytical modeling of the Earth's atmosphere and data observed from various space missions [10,14]. In order to obtain the radiance errors in roll and pitch, these radiance models are then used along with the model of sensor optics, signal processing and electronics. However, this procedure involves detailed knowledge of the sensor hardware. Hence, we approximate the noise due to radiance as an exponentially correlated noise in both the roll and pitch axes [15]. This model, though approximate, models the radiance errors as varying with time with a specified steady-state RMS value. The discrete time equation for horizon sensor noise due to radiance variation (w_ϕ and w_θ) is thus given as,

$$w_{\phi,k+1} = aw_{\phi,k} + l\sqrt{1-a^2}\nu_k \tag{12a}$$

$$w_{\theta,k+1} = aw_{\theta,k} + l\sqrt{1-a^2}\nu_k \tag{12b}$$

where l denotes the steady-state RMS value of radiance variation error and is taken as 0.06 deg [9], ν_k is the discrete time white noise with variance equal to unity, and the parameter a is defined in terms of the horizon sensor sample period (T_{hs}) and the correlation time of exponentially auto-correlated noise (τ_w),

$$a = \exp\left[\frac{-T_{hs}}{\tau_w}\right] \tag{13}$$

To account for the cyclic variation with latitude occuring every orbit, the parameter τ_w is selected as one-eighth of the orbital period. Sensor noise due to radiance variation for a sample simulation run is illustrated in Fig. 2. Errors due to sensor bias and static misalignment errors are added as constant bias (b_ϕ and b_θ) of magnitude 0.02 deg in each axis. Other random errors arising from the sensor hardware are modeled as discrete white (ν_ϕ and ν_θ) noise with its 3σ value as 0.042 deg. The measurements are sampled every 1 s. The values of parameters describing sensor bias and random errors are chosen based on brochure of Sodern Horizon Sensors [16].

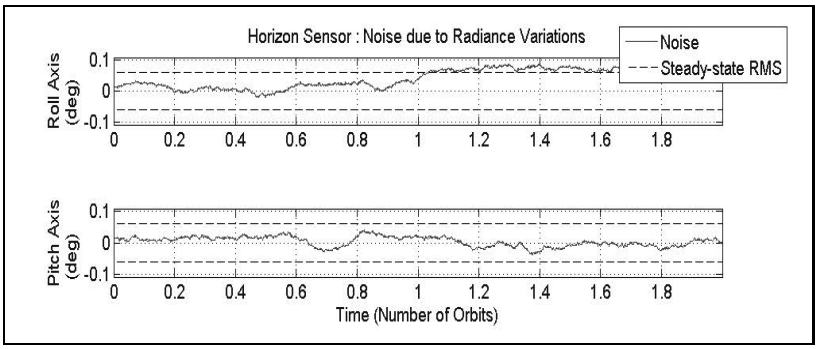

Fig. 2. Horizon sensor noise due to Radiance Variation

Horizon sensor measurement equations containing error from all the sources considered above can be written as,

$$\phi_{m,hs} = \left[\frac{1}{4}K\left(\theta_{\omega 0R} + \theta_{\omega 1R} - \theta_{\omega 0L} - \theta_{\omega 1L}\right)\right] + w_\phi + b_\phi + \nu_\phi \tag{14}$$

$$\theta_{m,hs} = \left[\frac{1}{4}\cos\xi\left(\theta_{\omega 0R} - \theta_{\omega 1R} + \theta_{\omega 0L} - \theta_{\omega 1L}\right)\right] + w_\theta + b_\theta + \nu_\theta \tag{15}$$

Oblateness Corrections. The horizon sensor errors described above contain both systemic as well as stochastic terms. To improve the accuracy of measurements, the systemic errors are predicted through analytical models, and subtracted from the measurements to mitigate the systemic errors. Earth's oblateness is one of the major systemic error which can be largely eliminated by proper modeling. Following the formulation of [11] oblateness corrections are calculated.

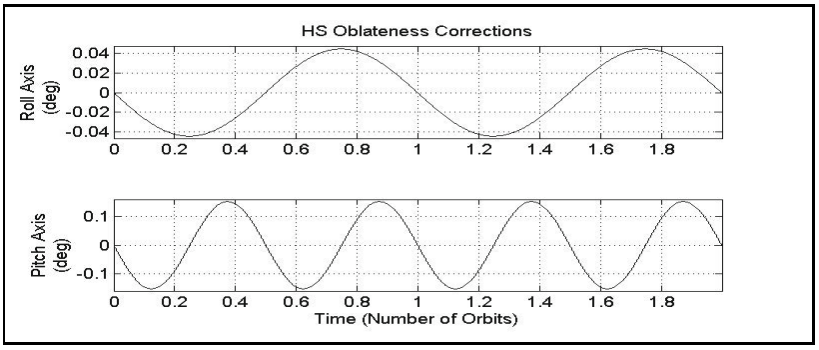

Fig. 3. Horizon Sensor : Oblateness Corrections

These oblateness corrections are added to the sensor measurements to remove the noise due to the Earth's oblateness. The variation of oblateness correction for orbit considered in our simulation is illustrated in Fig. 3. Corrections for other systemic errors, such as bias and residual noise due to radiance variation, can be done through on-board estimation techniques [17] or through post-processing of measurement residuals [9].

Horizon Sensor Parameters. A horizon sensor with clockwise scanning pattern is considered with realistic sensor parameters based on [9,16]. Table 3 lists the sensor parameters used during the simulation of the scanning type horizon sensors. Note that the sensor field-of-view is limited.

Table 3. Scanning Horizon Sensor Parameters

Parameter	Value	Units	Remark
ξ	20	deg	Canting Angle
δ_c	45	deg	Semi-cone Angle
FOV	25	deg	Field-of-View
l	0.06	deg	Radiance noise RMS (each axis)
b_{hs}	0.02	deg	Bias (each axis)
$3\sigma_{hs}$	0.042	deg	White noise (each axis)
T_{hs}	1	s	Sample Time

3 Development of Simulation

In order to validate and compare the attitude determination formulations, a six degree-of-freedom closed-loop simulation setup (Fig. 4), similar to that of Pratham student-satellite [8], is developed using MATLAB®-Simulink. A controller is included to observe the pointing accuracy obtained by the attitude determination and control sub-system.

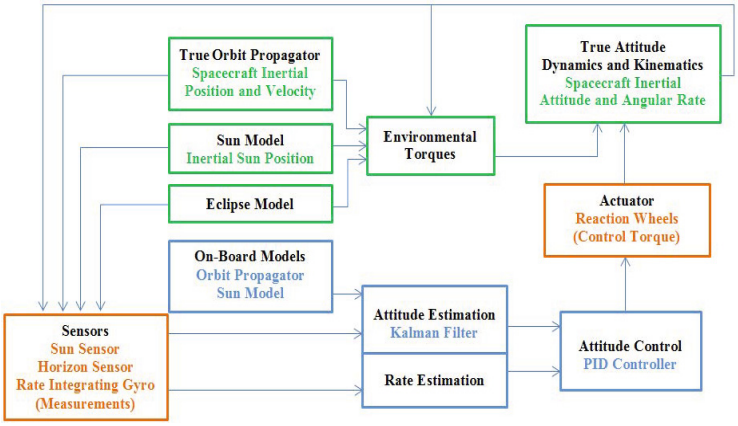

Fig. 4. Overview of Simulation

The design of the simulation is kept modular, so that it can be utilized to test different sets of sensors and attitude determination algorithms. The overall simulation sample rate is selected as 20 Hz, as it is sufficient to capture the system dynamics in simulation. Further, various sub-systems are simulated at different sample rates in order to account for their different sample times (see Table 4).

Standard equations for various simulation blocks as shown in Fig. 4 have been used [5]. Environmental torques due to gravity-gradient, solar radiation pressure and aerodynamic disturbance are considered. A sun-synchronous circular orbit

Table 4. Simulation rates of different sub-systems

Sub-system	Simulation Rate
True Attitude Dynamics	20 Hz
True Orbit Propagation	20 Hz
Sensors (Gyro)	10 Hz
Sensors (SS & HS)	1 Hz
On-board Models	10 Hz
Attitude Estimator	10 Hz
Controller	10 Hz

with altitude of 720 km and 98.28 deg inclination is considered, which is similar to that of the Oceansat-2 satellite [18]. Earth's gravity model which incorporates terms due to the Earth's oblateness upto J_2 zonal harmonics is used for orbit propagation [6]. The complete simulation setup has been validated with the help of conservation of angular momentum check in absence of external torques. Other models being standard, we here describe briefly the controller and rate estimation filter employed in our simulation.

3.1 Controller

A controller is required for the purpose of simulation, in order to observe the closed-loop performance of the attitude estimator. Here, we use a basic PID controller for our simulations. The gains of the PID controller are selected to obtain the desired damping ratio (ζ) of 0.707, and natural frequency (ω_n) corresponding to a time period of half minute, i.e., (0.5)(60)s. The parameter δ influences the integral gain, and helps to eliminate the steady-state error of the controller. The values of the normalized controller gains, for the listed specifications, are listed in Table 6.

Table 5. Controller Parameters

δ	0.7
ζ	0.707
ω_n	$\frac{2\pi}{(0.5)(60)} = 0.2094$

Table 6. Normalized Controller Gains

a_d	$(2+\delta)\zeta\omega_n$	0.3998
a_p	$\omega_n^2(1+2\delta\zeta^2)$	0.0746
a_i	$\delta\zeta\omega_n^3$	0.0045

Based on the values of controller gains the control torque vector is determined using the attitude and rate error, and satellite's moment of inertia, $\boldsymbol{I}$.

$$\mathbf{g}_{con} = \boldsymbol{I}\left(a_p\boldsymbol{\theta}_{err} + a_i\int \boldsymbol{\theta}_{err}dt + a_d\boldsymbol{\omega}_{err}\right) \tag{16}$$

$$\boldsymbol{\theta}_{err} = \boldsymbol{\theta}_{com} - \hat{\boldsymbol{\theta}} \tag{17}$$

$$\boldsymbol{\omega}_{err} = \boldsymbol{\omega}_{com} - \hat{\boldsymbol{\omega}} \tag{18}$$

Lastly, for all the simulation results presented the commanded attitude and angular rates align the spacecraft body frame with the LVLH frame.

3.2 Rate Filter

Estimate of inertial angular velocity of the spacecraft is required for control of the satellite. However, in the attitude estimation algorithms presented next, we only estimate the gyro drift rate bias and satellite attitude. Using the estimates of gyro drift rate bias the gyro measurement can be corrected for bias error; however, the measurements still include the random noise. The rate integrating gyros along with the above Kalman filter provide incremental attitude vector. Since the gyros work at a very high rate the incremental angles are related to $\boldsymbol{\omega}$ as follows

$$\Delta\hat{\boldsymbol{\theta}}_k = \Delta\boldsymbol{\varphi}_k - T_{gyro}\hat{\mathbf{b}}_k \tag{19}$$

$$\hat{\boldsymbol{\omega}}_{kf} \approx \frac{\Delta\hat{\boldsymbol{\theta}}_k}{T_{gyro}} \tag{20}$$

In order to remove the high frequency noise associated with above calculation of $\boldsymbol{\omega}$, a discrete low pass filter with bandwidth (ω_c) is used,

$$\hat{\boldsymbol{\omega}}_{k,lpf} = \frac{T_{gyro}\omega_c}{T_{gyro}\omega_c + 2}\hat{\boldsymbol{\omega}}_{k,kf} + \frac{T_{gyro}\omega_c}{T_{gyro}\omega_c + 2}\hat{\boldsymbol{\omega}}_{k-1,kf} - \frac{T_{gyro}\omega_c - 2}{T_{gyro}\omega_c + 2}\hat{\boldsymbol{\omega}}_{k-1,lpf} \tag{21}$$

This filtered estimate is used to arrive at the control torque, which results in a relatively smoother control action which is beneficial for actuator hardware. In our simulation the filter bandwidth is chosen as ten times that of the controller bandwidth.

4 Steady-State Kalman Filter

A steady-state three-axis Kalman Filter [2,7] is first presented for attitude determination. The filter provides the estimate of the spacecraft attitude and the gyro drift-rate bias. The gyro measurements, which are available at a very high rate, are used as the process model for the filter. The attitude sensors are used for correction of the attitude estimate and gyro drift-rate bias, and represent the measurement model. The prediction step using the rate integrating gyro measurements takes place at a higher rate, while the correction step is used only after a predetermined update interval (T_{up}).

Propagation equations, as they occur at a different rate, are described by using the subscript k. At the n-th gyro interval correction step is applied using the attitude sensors. In the following analysis, the indices $(-)$ and $(+)$ indicate the estimates prior to and post measurement updates from attitude sensors, respectively. The choice of update interval depends on the sensor error characteristics, sensor sampling rate and required pointing accuracy, and is discussed subsequently.

4.1 Prediction

Based on the gyro measurement model (Eq. 3) the propagation equations for the filter, which utilize the gyro measurements $\Delta\boldsymbol{\varphi}$, are given as:

$$\Delta\hat{\boldsymbol{\theta}}_k = \Delta\boldsymbol{\varphi}_k - T_{gyro}\hat{\mathbf{b}}_k \tag{22}$$

$$\hat{\mathbf{b}}_k = \hat{\mathbf{b}}_{k-1} \tag{23}$$

In order to obtain incremental inertial attitude from the attitude estimates, following propagation equations for the direction cosine matrix are used [19],

$$\hat{\mathrm{C}}_{k,I} = \hat{\mathrm{C}}_{k,k-1}\hat{\mathrm{C}}_{k-1,I} \tag{24}$$

$$\hat{\mathrm{C}}_{k,k-1} = \mathbf{I}_{3\times3} - \Delta[\hat{\boldsymbol{\theta}}^{\times}] + \frac{\Delta\hat{\boldsymbol{\theta}}_k\Delta\hat{\boldsymbol{\theta}}_k^T - \|\Delta\hat{\boldsymbol{\theta}}_k\|^2\mathbf{I}_{3\times3}}{2} \tag{25}$$

4.2 Steady-State Kalman Gains

To obtain the correction equations, we first need to determine the Kalman Filter gains. The gains depend on innovation covariance, error covariance of the process and measurement noise. Following the steady-state analysis of [2], the Kalman Gains for each axis are represented using three non-dimensional parameters - dependent on the sensor errors $\sigma_u, \sigma_v, \sigma_n$ and the correction update interval T_{up} - characterizing the readout noise ($S_e = \frac{\sigma_e}{\sigma_n}$), random-walk noise ($S_u = \frac{T_{up}^{3/2}\sigma_u}{\sigma_n}$), and drift angle $S_v = \frac{T_{up}^{1/2}\sigma_v}{\sigma_n}$. Based on the steady-state covariance analysis, the steady-state Kalman Filter gains are,

$$K_{hs} = (\zeta\sigma_n)^{-2}\begin{bmatrix} P_{\theta\theta}(-) \\ P_{\theta b}(-) \\ P_{\theta\varphi}(-) \end{bmatrix} = \begin{bmatrix} 1-\zeta^{-2} \\ (\zeta T_{up})^{-1}S_u \\ (S_e/\zeta)^2 \end{bmatrix} \tag{26}$$

where,

$$\gamma = (1 + S_e^2 + \frac{1}{4}S_v^2 + \frac{1}{48}S_u^2)^{\frac{1}{2}} \tag{27}$$

$$\zeta = \gamma + \frac{1}{4}S_u + \frac{1}{2}(2\gamma S_u + S_v^2 + \frac{1}{3}S_u^2)^{\frac{1}{2}} \tag{28}$$

4.3 Correction

In order to utilize the attitude sensors (sun and horizon sensors) the measurements of roll, pitch, and yaw, are transformed and represented as,

$$\hat{\mathrm{C}}_{n.att,I} = \left(\mathbf{I}_{3\times3} - [\boldsymbol{\nu_{att}}^{\times}]\right)\hat{\mathrm{C}}_{n,I} \tag{29}$$

wherein the subscript *'att'* refers to both the horizon and sun sensors and $\boldsymbol{\nu}_{att}$ quantifies the total noise in the attitude measurements. In order to obtain a three-axis equivalent of the small angle error residual, we observe that

$$\theta_{att} - \hat{\theta}_0\,(-) \Leftrightarrow \hat{\mathrm{C}}_{n.att,I}\hat{\mathrm{C}}_{I,n.gyro} \tag{30a}$$

$$\approx \mathbf{I}_{3\times 3} - [\boldsymbol{\nu}_{att} - \hat{\boldsymbol{\nu}}_{n.gyro}]^{\times} \tag{30b}$$

$$= \mathbf{I}_{3\times 3} - [\boldsymbol{\nu}_{\boldsymbol{att/gyro}}{}^{\times}] \tag{30c}$$

Hence, $\boldsymbol{\nu}_{att/gyro}$ characterizes the required difference, and can be obtained in terms of the available matrices $\hat{\mathrm{C}}_{n.att,I}$ (from measurement) and $\hat{\mathrm{C}}_{I,n.gyro}$ (from estimator),

$$\boldsymbol{\nu}^{\times}_{att/gyro} = \mathbf{I}_{3\times 3} - \hat{\mathrm{C}}_{n.att,I}\hat{\mathrm{C}}_{I,n.gyro} \tag{31}$$

The correction equation in terms of $\boldsymbol{\nu}_{att/gyro}$ for attitude and bias are given as,

$$\boldsymbol{\nu}_{att/update} = \begin{bmatrix}(1-\zeta_x^{-2})\nu_{att/gyro,x}\\(1-\zeta_y^{-2})\nu_{att/gyro,y}\\(1-\zeta_z^{-2})\nu_{att/gyro,z}\end{bmatrix} \tag{32}$$

$$\hat{\mathrm{C}}_{0.gyro,I}(+) = (\mathbf{I}_{3\times 3} - [\boldsymbol{\nu}_{att/update}]^{\times})\hat{\mathrm{C}}_{n.gyro,I} \tag{33}$$

$$\hat{\mathbf{b}}_0(+) = \hat{\mathbf{b}}_0(-) - \begin{bmatrix}S_{u,x}(\zeta_x T_{up})^{-1}\nu_{att/gyro,x}\\S_{u,y}(\zeta_y T_{up})^{-1}\nu_{att/gyro,y}\\S_{u,z}(\zeta_z T_{up})^{-1}\nu_{att/gyro,z}\end{bmatrix} \tag{34}$$

The filter thus provides estimates of inertial attitude which can be transformed to other frames as per the requirement of the attitude control sub-system. The estimates of bias are used to correct the gyro measurement. Note that since the KF gains in the three axes are independent of each other, asynchronous sun and horizon sensor measurements can also be used by the steady-state Kalman filter. Next, we discuss the initialization of the filter, selection of the update parameter and the filter's simulated performance.

4.4 Initialization

To reduce the filter transients, the filter should be initialized with the best attitude estimate available. This *a priori* estimate can be obtained from the Sun and horizon sensor measurements. These measurements are used to initialize the attitude states of the filter. The drift bias states of the filter should be initialized with the drift bias value specified in the specification sheet or as obtained through ground testing of the gyro.

4.5 Update Interval

In the above formulation, all but one variables influencing Kalman gains are dependent on the sensor characteristic. The parameter T_{up} also influences Kalman Gains, and can be chosen by the designer. The achievable values of T_{up} will be limited due to the sample time of attitude sensors (T_{hs} and T_c), and computational capability of the on-board computer. Based on steady-state covariance

analysis, variation of achievable estimate covariance with respect to T_{up} is obtained, as shown in Figs. 5-6. Both pre- and post-update covariance estimates at steady-state and corresponding standard deviation of attitude sensor errors are shown. Using the plots, the parameter T_{up} is chosen as 2s, since it provides estimation accuracy of ~ 0.01 deg at steady-state.

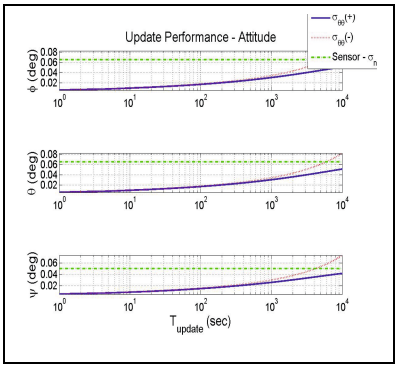

Fig. 5. T_{up} anlaysis : Attitude

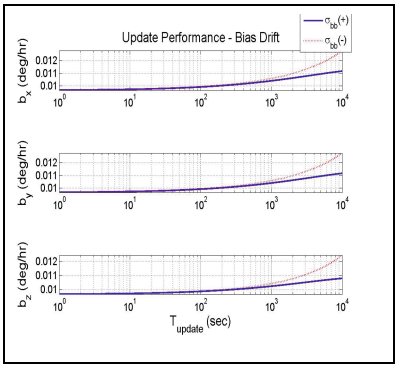

Fig. 6. T_{up} anlaysis : Gyro Bias

4.6 Estimator Performance

The results of the three-axes attitude determination algorithm developed above are now presented. The filter is propagated at a rate of 10 Hz and the attitude sensor measurement corrections are effected every 2s. The rate low-pass filter with cut-off frequency $\omega_c = 0.32$ Hz is used. Horizon sensor measurements are corrected for oblateness prior to being used in the filter and no gyro misalignments are considered. Initial estimation errors, tabulated in Table 7, have been included as per section 4.4.

Table 7. Initial Estimation Errors

Attitude Estimation Error(deg)		
ϕ	θ	ψ
0.1	0.1	0.1
Drift Bias Estimation Error (deg/hr)		
b_x	b_y	b_z
0.03	0.03	0.03

Test Case: As a theoretical test case, we observe the performance of the filter in presence of white noise in attitude sensors, where the model in the Kalman filter completely matches with the measurements. The estimation performance is within the predicted bounds (Figs. 7-8); however, long duration transients

(up to 20% of the orbit period) persist before the steady-state is arrived at. Due to the coupling between the roll and yaw axis, and propagation due to the gyro measurements, performance in the eclipse region is also satisfactory.

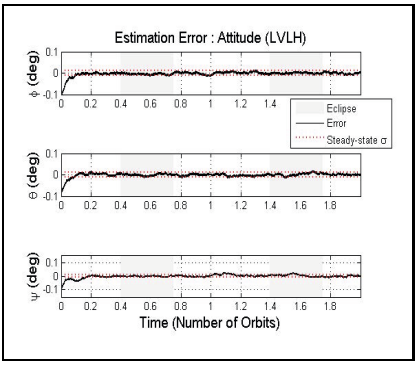

Fig. 7. Steady-state KF with white measurement noise : Attitude

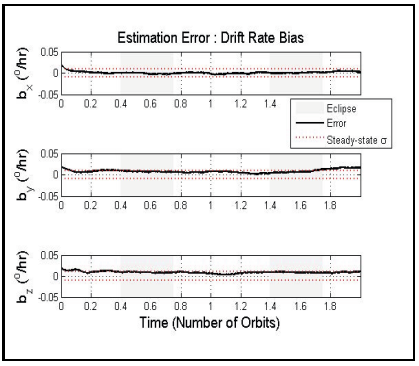

Fig. 8. Steady-state KF with white measurement noise : Gyro Bias

Performance with Realistic Measurement Errors: Next, using the estimator parameters specified earlier, we obtain the performance of the steady-state KF in presence of all sensor errors except gyro misalignments. As observed in Figs. 9-10, the estimation performance has degraded considerably as compared to the theoretical test case. However, this is expected as the bias and radiance variations in horizon sensor measurements are not being compensated for in the estimation algorithm.

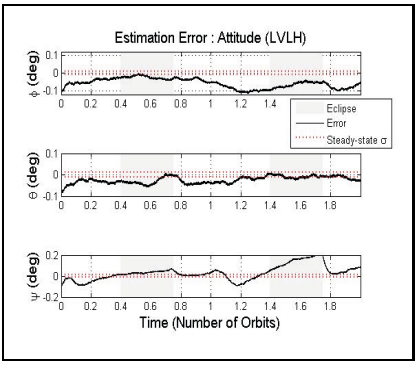

Fig. 9. Steady-state KF : Attitude

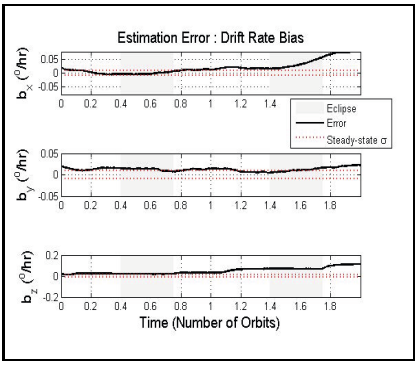

Fig. 10. Steady-state KF : Gyro bias

5 Extended Kalman Filter

This section briefly describes the quaternion-based extended Kalman filter (EKF) of Lefferts, Markley and Shuster [3] for satellite attitude determination. As with the steady-state KF, this filter too estimates the satellite attitude and gyro drift rate bias.

5.1 Formulation

The quaternion-based EKF estimates the attitude quaternion ($\mathbf{q}_{BI}$, 4 elements) and gyro bias ($\mathbf{b}$, 3 elements) resulting in seven states. However, the covariance propagation is achieved through error state to avoid the quaternion singularity. The error states for quaternion ($\delta\mathbf{q} = \mathbf{q} \otimes \hat{\mathbf{q}}^{-1}$) and bias ($\boldsymbol{\Delta b} = \mathbf{b} - \hat{\mathbf{b}}$) result in a six-element state vector: $\boldsymbol{\Delta x} = [\delta\mathbf{q}, \boldsymbol{\Delta b}]'$. Process model for error state is then given as $\boldsymbol{\Delta \dot{x}} = \mathrm{F}\boldsymbol{\Delta x} + \mathrm{G}\mathbf{w}$, where,

$$\mathrm{F} = \begin{bmatrix} -[\boldsymbol{\omega}^{\times}] & -1/2\mathbf{I}_{3\times3} \\ \mathbf{0}_{3\times3} & \mathbf{0}_{3\times3} \end{bmatrix} \tag{35}$$

$$\mathrm{G} = \begin{bmatrix} -1/2\mathbf{I}_{3\times3} & \mathbf{0}_{3\times3} \\ \mathbf{0}_{3\times3} & \mathbf{I}_{3\times3} \end{bmatrix} \tag{36}$$

$$\mathbf{w} = \begin{bmatrix} \boldsymbol{\eta_v} & \boldsymbol{\eta_u} \end{bmatrix}' \tag{37}$$

The development of the quaternion EKF in [3] provides freedom while using the attitude sensors, in the sense that the measurements can be used either as scalar angles or reference vectors. Through simulation it was observed that use of either approaches produces similar performance; hence, here we present only one of them. Sensor models presented earlier represent the measurement models. Here, we list the measurement noise covariance (R) and sensitivity (H) matrices corresponding to the two attitude sensors,

Sun Sensor

$$\mathrm{R}_k = E[\mathbf{v}_k'\mathbf{v}_k] = \sigma_c^2(\mathbf{I}_{3\times3}) \tag{38}$$

$$\mathrm{H}_k = \begin{bmatrix} 2(\mathbf{r}_1 \times \hat{\mathbf{z}}_k)' & \mathbf{0}_{1\times3} \\ 2(\mathbf{r}_2 \times \hat{\mathbf{z}}_k)' & \mathbf{0}_{1\times3} \\ 2(\mathbf{r}_3 \times \hat{\mathbf{z}}_k)' & \mathbf{0}_{1\times3} \end{bmatrix} \tag{39}$$

where, $\mathbf{r}_i = [\delta_{i1}, \delta_{i2}, \delta_{i3}]'$, the symbol δ_{ij} representing the Kronecker delta; and $\hat{\mathbf{z}}_k (= \hat{\mathbf{s}}_B = [\mathrm{C}(\hat{\mathbf{q}})]\mathbf{s}_I)$ corresponds to the modeled sun vector in the body frame. The sensitivity matrix H_k is derived through application of the corresponding general expressions provided in (Eq. 151-157) of [3].

Horizon Sensor

$$\mathrm{R}_k = \begin{bmatrix} \sigma_\theta^2 & 0 \\ 0 & \sigma_\phi^2 \end{bmatrix} \tag{40}$$

$$\mathrm{H}_k = \begin{bmatrix} 2(\mathbf{r}_1 \times \hat{\mathbf{z}}_k)' & \mathbf{0}_{1\times3} \\ 2(\mathbf{r}_2 \times \hat{\mathbf{z}}_k)' & \mathbf{0}_{1\times3} \end{bmatrix} \tag{41}$$

where $\hat{\mathbf{z}}_k$ corresponds to the modeled value of the nadir vector in the body frame; and horizon sensor measurement is represented as $[-\theta_m, \phi_m]'$ to correspond to the definition of the nadir vector. As expected these measurements depend only on the attitude and not on the gyro bias. For further details of this filter and the standard Kalman Filter equations the reader is directed to reference [3].

5.2 Estimator Performance

We present the performance of the quaternion-based EKF using similar measurement models and parameters as to that for the steady-state KF. As the measurements from different sensors need not be synchronous, each measurement update is applied independently, using Murell's approach [20]. While calculating filter gains we need to specify P_0. When the sun and horizon sensors are used to provide the initial estimates, value of P_0 corresponding to the accuracy of these sensors is used. The initial drift bias state covariances can be obtained from ground testing of the gyro.

Test Case: The Kalman filter is optimal in presence of measurement errors being white noise. Hence, similar to the case of steady-state KF, as a theoretical test case, we first observe the performance of the EKF in presence of only white noise in attitude sensors. The absence of yaw (sun sensor) measurements, during the eclipse phase, results in increased state covariance in yaw estimates. Due to the exact correspondence between the measurement noise and its model being white, the assumptions of EKF are satisfied, resulting in the expected estimation performance, shown in Figs. 11-12.

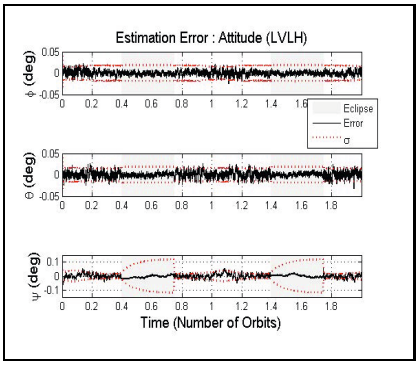

Fig. 11. EKF (white noise) : Attitude

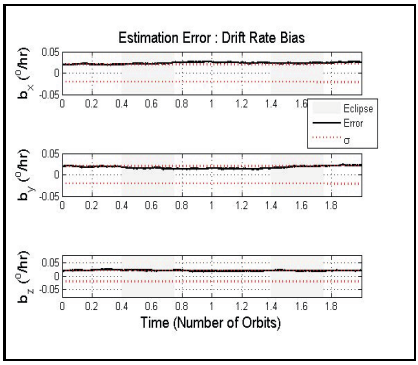

Fig. 12. EKF : Gyro bias

Performance with Realistic Measurement Errors: Having verified the filter through a simplified measurement model, we observe its performance in presence of the complete measurement models except for misalignments. Similar to

the case of steady-state KF, the performance of the filter deteriorates. The observed estimation accuracy in presence of colored noise and bias in measurement is given as seen in Figs. 13-14.

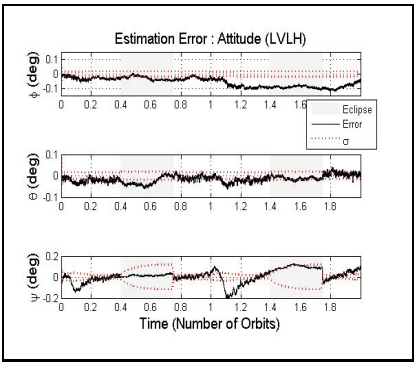

Fig. 13. EKF : Attitude

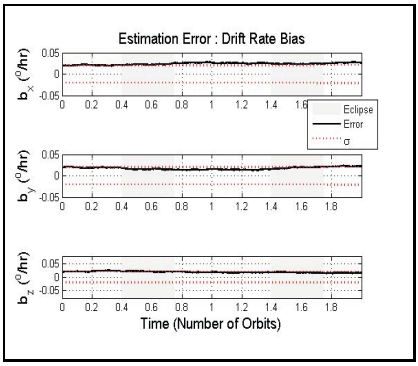

Fig. 14. EKF : Gyro bias

6 Estimation of Additional States

The horizon sensor measurements used in both the steady-state KF and quaternion-based EKF described earlier contain errors such as biases and radiance variations, which are not just white noise. These filters, however, work under the assumption that the errors entering the measurement model are white - resulting therefore in sub-optimal estimation performance. Better estimates of the attitude requires augmentation of the state vector, albeit without any additional measurements. This may result in the system becoming unobservable, degrading the attitude performance. Attempts to estimate biases of attitude sensors [17] and the noise due to radiance variation [21] have been reported earlier in the literature, and mixed results have been obtained. Hence, the augmented state vector filter should be implemented only after verifying the performance of the estimator through analysis and simulation. We proceed with the state vector augmentation for the quaternion-based EKF instead of the steady- state KF, due to its relatively straight-forward formulation and ease of implementation. A similar approach of state vector augmentation for estimation of misalignment and scale factor errors has been developed by Pittelkau.

6.1 Horizon Sensor Error Estimation

The state vector is augmented with the noise terms corresponding to the horizon sensor radiance error $(w_\phi,\ w_\theta)$: $\mathbf{x}(t) = [\mathbf{q}_{BI}, \boldsymbol{\Delta b}_g, w_\phi, w_\theta]'$. The discrete-time model for radiance errors in roll and pitch is given by Eq. (12a-12b). This can be represented as a differential equation,

$$\dot{w_\phi}(t) = -\beta w_\phi + \eta_{\phi,w} \tag{42}$$

$$\dot{w_\theta}(t) = -\beta w_\theta + \eta_{\theta,w} \tag{43}$$

where the parameter β and the PSD of η are obtained by comparing the continuous model with the discrete-time equation: $\beta = \frac{1}{\tau_w}$, PSD of $\eta_{\phi,w}$and $\eta_{\theta,w} = \frac{l^2(1-a^2)}{T_{hs}}$. The evolution of these error parameters is independent of the attitude and gyro bias, and the same is reflected in the modified process model,

$$\frac{d}{dt}\begin{bmatrix} \mathbf{q}_{BI} \\ \boldsymbol{\Delta b}_g \\ w_\phi \\ w_\theta \end{bmatrix} = \begin{bmatrix} -[\boldsymbol{\omega}^\times] & -1/2\mathbf{I}_{3\times3} & \mathbf{0}_{3\times1} & \mathbf{0}_{3\times1} \\ \mathbf{0}_{3\times3} & \mathbf{0}_{3\times3} & \mathbf{0}_{3\times1} & \mathbf{0}_{3\times1} \\ \mathbf{0}_{1\times3} & \mathbf{0}_{1\times3} & -\beta & 0 \\ \mathbf{0}_{1\times3} & \mathbf{0}_{1\times3} & 0 & -\beta \end{bmatrix} \begin{bmatrix} \mathbf{q}_{BI} \\ \boldsymbol{\Delta b}_g \\ w_\phi \\ w_\theta \end{bmatrix} + \begin{bmatrix} -1/2\boldsymbol{\eta_v} \\ \boldsymbol{\eta_u} \\ \eta_{\phi,w} \\ \eta_{\theta,w} \end{bmatrix} \tag{44}$$

Propagation equation for the quaternion and bias is the same as for the filter described earlier. The propagation for the radiance variation is done using the discrete counterpart of the process model described above. Sun sensor measurement equations and corresponding noise covariance (Eq. 38) remains the same. Horizon sensor measurements are corrected for noise due to oblateness. In the current formulation, an estimate of the horizon sensor noise due to radiance variation is developed so as to subtract it from the horizon sensor measurements. The corresponding sensitivity matrix is given as,

$$\mathrm{H}_k = \begin{bmatrix} 2(\mathbf{r}_1 \times \hat{\mathbf{z}}_k)' & \mathbf{0}_{1\times3} & 0 & -1 \\ 2(\mathbf{r}_2 \times \hat{\mathbf{z}}_k)' & \mathbf{0}_{1\times3} & 1 & 0 \end{bmatrix} \tag{45}$$

Radiance Noise Estimation. The initial estimate of the attitude and gyro bias are specified to be the same as before, whereas since no estimate of residual error due to radiance variation is available its initial value is taken as zero. The steady-state RMS value of radiance noise is used to define P_0, the initial state covariance. As seen in Figs. 15-16, the estimation error of the radiance noise is within the covariance bounds. However, the predicted bounds for the most part of the orbit are the same as l, the steady-state RMS of the radiance noise.

Although the radiance noise is estimated to certain accuracy, the improvements in attitude estimation are not significant even with the application of this modified filter (Fig. 6.1). Similar results were reported in [21] wherein with real attitude data a similar augmented filter was able to estimate the radiance noise but improved the attitude estimation performance only marginally.

Bias Estimation. Apart from radiance noise, the horizon sensor measurements also have a constant bias which may arise due to sensor electronics or static misalignment. Since our filter currently does not estimate the bias, the attitude estimate might improve with estimation of this bias, even though the magnitude of this bias is relatively smaller than the radiance noise. Hence, we try to estimate the horizon sensor bias using the augmented filter, instead of the radiance noise.

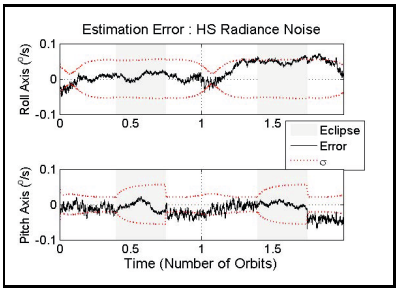

Fig. 15. Horizon Sensor Radiance Noise : Estimation Error

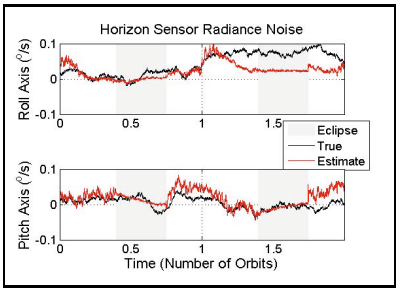

Fig. 16. Horizon Sensor Radiance Noise : True v/s Estimate

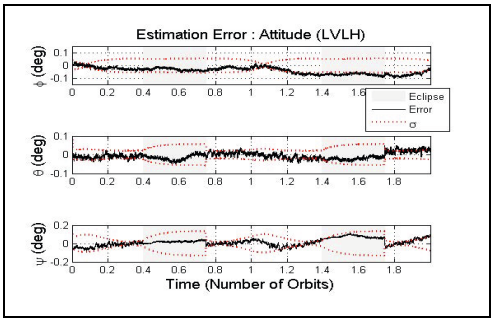

Fig. 17. Effect of Radiance Estimation : Attitude

The formulation to estimate radiance noise can be adapted to estimate horizon sensor bias, by choosing the parameter β in the process model of the filter as zero. The filter is initialized similar to the case of radiance estimation. The horizon sensor bias estimation performance is portrayed in Figs. 18-19.

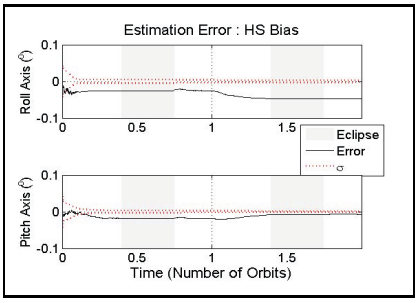

Fig. 18. Horizon Sensor Bias : Estimation Error

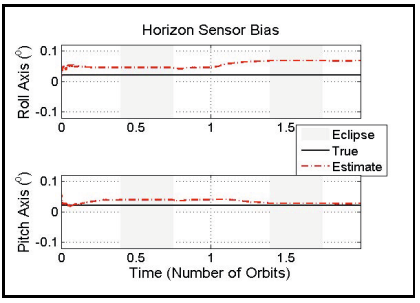

Fig. 19. Horizon Sensor Bias : True v/s Estimate

Improvements in attitude estimation accuracy are obtained due to estimation of the horizon sensor bias. As seen in Fig. 20, the attitude estimation accuracy is generally within the predicted covariance, and yaw estimates do not degrade much during eclipse.

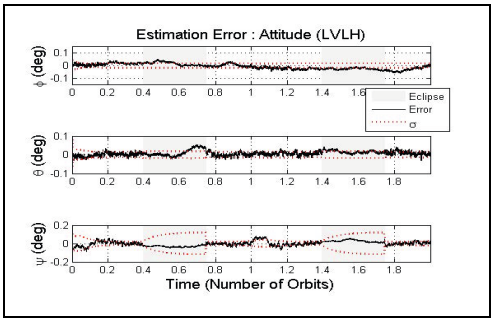

Fig. 20. Effect of Bias Estimation : Attitude

6.2 Misaligned Sensors

In the simulation discussed till now, no sensor misalignments were considered. Presence of misalignment in either the gyro or the attitude sensors may result in incorrect estimates of both the attitude and gyro drift rate bias. Both batch and sequential misalignment estimation method exist in the literature. Here, we consider application of the misalignment estimation Kalman filter developed by Pittelkau [4], which is called the Alignment Kalman Filter (AKF). This filter is suited for on-board real time estimation of sensor misalignments and scale factor errors.

The AKF, too, is an augmentation of the quaternion-based EKF. The augmented state vector is given as $\mathbf{x} = [\boldsymbol{\delta q}_v, \boldsymbol{\Delta b}_g, \boldsymbol{\delta}_g, \mathbf{b}_{HS}]'$, where, the parameter $\boldsymbol{\delta}_g$ $(= [\lambda_x, \delta_{yz}, \delta_{zy}, \delta_{xz}, \lambda_y, \delta_{zx}, \delta_{xy}, \delta_{yx}, \lambda_z]')$ denotes the gyro misalignments and scale factor terms, and $\mathbf{b}_{HS}$ $(= [b_\phi, b_\theta]')$ denotes the two components of horizon sensor bias . The alignment Kalman filter, thus, attempts to estimate additional states - misalignment of sensors - along with the attitude and sensor biases. However, the number of measurements used for correction of the state vector still remain the same. Naturally, this causes concerns of observability of the state vector and potential degradation of the estimate. In order to make the system observable, and prevent ill effects of state augmentation, in-flight attitude maneuvers are performed. These maneuvers are of higher frequency then the spacecraft dynamics, and for on-board implementation require capable actuators. The system is made observable by subjecting the spacecraft to

non-harmonic sinusoidal angular rates. Hence, the rate command for the attitude controller is modified to be as,

$$\boldsymbol{\omega}_{BO}^{B} = (0.05\,\mathrm{deg}\,/\,\mathrm{sec}) \begin{bmatrix} \sin[2\pi(0.0100)] \\ \sin[2\pi(0.0085)] \\ \sin[2\pi(0.0080)] \end{bmatrix} \tag{46}$$

The process model for the above state vector is given as,

$$\frac{d}{dt}\begin{bmatrix} \mathbf{q}_{BI} \\ \boldsymbol{\Delta b}_g \\ \boldsymbol{\delta}_g \\ \mathbf{b}_{HS} \end{bmatrix} = \begin{bmatrix} -[\boldsymbol{\omega}^{\times}] & -1/2\mathbf{I}_{3\times3} & 1/2\Omega_g & \mathbf{0}_{3\times2} \\ \mathbf{0}_{3\times3} & \mathbf{0}_{3\times3} & \mathbf{0}_{3\times9} & \mathbf{0}_{3\times2} \\ \mathbf{0}_{9\times3} & \mathbf{0}_{9\times3} & \mathbf{0}_{9\times9} & \mathbf{0}_{9\times2} \\ \mathbf{0}_{2\times3} & \mathbf{0}_{2\times3} & \mathbf{0}_{2\times9} & \mathbf{0}_{2\times2} \end{bmatrix} \begin{bmatrix} \mathbf{q}_{BI} \\ \boldsymbol{\Delta b}_g \\ \boldsymbol{\delta}_g \\ \mathbf{b}_{HS} \end{bmatrix} + \begin{bmatrix} -1/2(\mathbf{I}_{3\times3} + \mathrm{M})\boldsymbol{\eta_v} \\ \boldsymbol{\eta_u} \\ \boldsymbol{\eta_g} \\ \boldsymbol{\eta_b} \end{bmatrix} \tag{47}$$

where, M denotes the gyro misalignment and scale factor matrix,

$$\mathrm{M} = \begin{bmatrix} \lambda_x & -\delta_{yz} & \delta_{zy} \\ \delta_{xz} & \lambda_y & -\delta_{zx} \\ -\delta_{xy} & \delta_{yx} & \lambda_z \end{bmatrix} \tag{48}$$

and Ω_g is defined in terms of the inertial rates,

$$\Omega_g = \begin{bmatrix} \omega_x & -\omega_y & \omega_z & 0 & 0 & 0 & 0 & 0 & 0 \\ 0 & 0 & 0 & \omega_x & \omega_y & -\omega_z & 0 & 0 & 0 \\ 0 & 0 & 0 & 0 & 0 & 0 & -\omega_x & \omega_y & \omega_z \end{bmatrix} \tag{49}$$

The propagation equations for $\boldsymbol{\delta}_g$ and $\mathbf{b}_{HS}$ is the same as that of the $\boldsymbol{\Delta b}_g$ due to analogous continuous time equations. The propagation of the full quaternion is also done similar to that of the 6-state EKF, except that rate-integrating gyro measurements are compensated not just for drift rate bias but also misalignments and scale factors using available estimates. The measurement sensitivity matrix is expanded to account for the additional states; for instance, for horizon sensor the sensitivity matrix is given as,

$$\mathrm{H}_k = \begin{bmatrix} 2(\mathbf{r}_1 \times \hat{\mathbf{z}}_k)' & \mathbf{0}_{1\times3} & \mathbf{0}_{1\times9} & 0 & -1 \\ 2(\mathbf{r}_2 \times \hat{\mathbf{z}}_k)' & \mathbf{0}_{1\times3} & \mathbf{0}_{1\times9} & 1 & 0 \end{bmatrix} \tag{50}$$

When the spacecraft is subjected to sinusoidal rate maneuvers, as specified in Eq. 46, the misalignment states are expected to become observable, resulting in improvement in attitude estimation performance. Further, the attitude and gyro drift rate bias performance is within the Kalman filter covariance bounds (Figs. 21-22).

The estimation of scale factors and misalignment in all the three axes is possible. Within two orbits the scale factor and miaslignment estimation errors achieve steady-state (Figs. 23-24), after which the maneuvers are terminated and normal spacecraft operation is resumed.

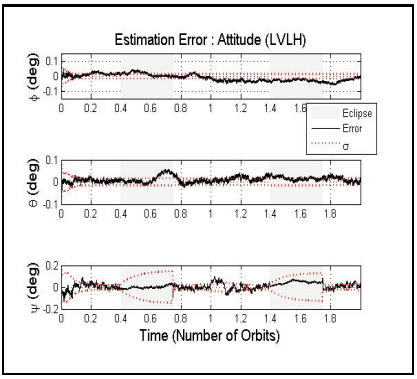

Fig. 21. AKF : Attitude

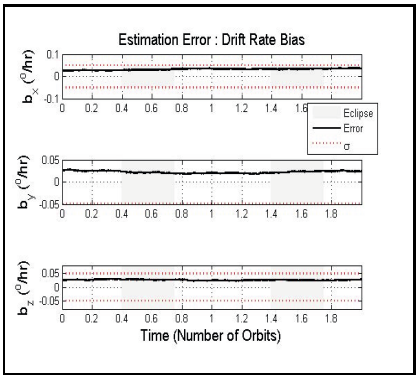

Fig. 22. AKF : Gyro Bias

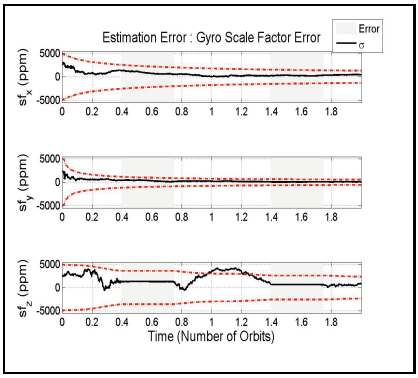

Fig. 23. Gyro Scale Factors : Estimation Error

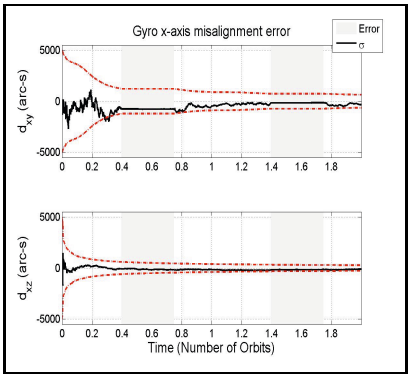

Fig. 24. Gyro Misalignment (x-axis) : Estimation Error

7 Conclusions and Comments

Sequential on-board attitude estimation algorithms for the sensor suite - sun sensor, horizon sensor and gyros - are studied, analyzed and simulated. As the attitude estimation algorithms are tested through simulation, an effort is made to consider detailed models of sensors and to test the algorithms in presence of realistic sensor errors. A standard, realistic model of rate-integrating gyro is used which includes time varying drift-rate bias, static misalignment, scale factor errors and quantization noise. Horizon sensor modeling includes effects of Earth's oblateness, atmospheric radiance, bias and electronic noise. An approximate model of noise due to atmospheric radiance, treating it as an exponentially auto-correlated noise, is considered. A modular six degree-of-freedom closed-loop simulation has been developed, and performance of the attitude estimation algorithms using this simulation is presented.

Two attitude estimation algorithms - the DCM-based steady-state KF and quaternion-based EKF - are simulated. Modifications in the standard algorithms have been made, to customize them for the sensors under consideration. The steady-state filter is observed to work for the current sensor suite if only white noise is present in the attitude sensors. Hence, the steady-state KF, which is computationally efficient, may be a preferred choice in the case of the sensors primarily exhibiting such noise characteristics, such as the star trackers [7]. Further, depending on sensor error characteristics and required estimation accuracy, the steady-state KF may not be suitable during the eclipse phase of the orbit.

The quaternion-based EKF, too, in its original form works only for attitude sensors with white noise. Hence, there is a need to estimate other errors in the attitude sensors through augmentation of the state vector. The quaternion-based EKF offers a natural framework for estimation of additional states. Through estimation of horizon sensor bias, but not that of radiance noise, improvement in estimator performance is observed. Even during the eclipse phase of the orbit, when the sun sensor measurements are not available, the filter performance is satisfactory. The performance of steady-state KF may also be improved by estimation of horizon sensor bias; however, the quaternion-based EKF offers a simpler way of augmenting the state vector and can better handle asynchronous measurements. Hence, we recommend the use of the quaternion-based EKF with augmented state vector. Lastly, to account for sensor misalignment and scale factor errors, the alignment Kalman filter is studied and simulated. Due to satellite maneuvers, the AKF is able to estimate the misalignment parameters, resulting in desired attitude estimation performance.

References

1. Markley, F.L.: Spacecraft attitude determination methods. In: Israel Annual Conference on Aerospace Sciences (2000)
2. Markley, F.L., Reynolds, R.G.: Analytic steady-state accuracy of a spacecraft attitude estimator. Journal of Guidance, Control, and Dynamics 23(6), 1065–1067 (2000)
3. Leerts, E.J., Markley, F.L., Shuster, M.D.: Kalman ltering for spacecraft attitude estimation. Journal of Guidance 5(5), 417–429 (1982)
4. Pittelkau, M.E.: Kalman filtering for spacecraft system alignment calibration. Journal of Guidance, Control, and Dynamics 24(6), 1187–1195 (2001)
5. Wertz, J.R. (ed.): Spacecraft Attitude Determination and Control. Computer Sciences Corporation (1978)
6. Sidi, M.J.: Spacecraft Dynamics and Control. Cambridge University Press (1997)
7. Hablani, H.B.: Autonomous inertial relative navigation with sight-line-stabilized integrated sensors for spacecraft rendezvous. Journal of Guidance, Control, and Dynamics 32(1) (2009)
8. Joshi, J., et al.: Conceptual design report - ADCS, PRATHAM. Technical report, Indian Institute of Technology Bombay (2009)
9. Alex, T.K., Shrivastava, S.K.: On-board corrections of systematic errors of earth sensors. IEEE Transactions on Aerospace and Electronic Systems 25(3), 373–379 (1989)

10. Alex, T.K., Seshamani, R.: Generation of infrared earth radiance for attitude determination. Journal of Guidance, Control, and Dynamics 12(2), 257–277 (1989)
11. Hablani, H.B.: Roll/pitch determination with scanning horizon sensors - oblateness and altitude corrections. Journal of Guidance, Control, and Dynamics 18(6), 1355–1364 (1995)
12. Tekawy, J.A., Wang, P., Gray, C.W.: Scanning horizon sensor attitude corrections for earth oblateness. Journal of Guidance, Control and Dynamics 19(3), 706–708 (1996)
13. Hashmall, J.A., Sedlak, J., Andrews, D., Luquette, R.: Empirical correction for earth sensor horizon radiance variation. In: Proceedings, AAS/GSFC 13th International Symposium on Space Flight Dynamics, Goddard Space Flight Center,Greenbelt, Maryland (May 1998)
14. Phenneger, M.C., Singhal, S.P., Lee, T.H., Stengle, T.H.: Infrared horizon sensor modeling for attitude determination and control: analysis and mission experience. NASA technical memorandum. National Aeronautics and Space Administration,Scientific and Technical Information Branch (1985)
15. Crassidis, J.L., Markley, F.L., Kyle, A.M., Kull, K.: Attitude determination improvements for GOES. In: Proceedings, Flight Mechanics/ Estimation Theory Symposium, Goddard Space Flight Center, Greenbelt, Maryland, NASA Conference Publication 3333, pp. 161–175 (May 1996)
16. STD 16, EADS Sodern Earth Sensor Brochure, `www.sodern.com/sites/docs_wsw/RUB_52/STD16.pdf`
17. Deutschmann, J., Bar-Itzhack, I.Y.: Extended kalman filter for the attitude estimation of the earth radiation budget satellite. In: Proceedings, Flight Me chanics/Estimation Theory Symposium, Goddard Space Flight Center, Greenbelt, Maryland, NASA Conference Publication 3050, pp. 333–346 (1989)
18. ISRO Oceansat-2 Brochure. Oceansat-2-Brochure-1.pdf, `http://www.isro.org/pslv-c14/pdf/`
19. Hughes, P.C.: Spacecraft Attitude Dynamics. Dover Publications (2004)
20. Crassidis, J., Junkins, J.: Optimal Estimation of Dynamic Systems. Chapman & Hall/CRC Applied Mathematics and Nonlinear Science Series. Chapman &Hall/CRC (2004)
21. Sedlak, J.: Improved earth sensor performance using a sequentially correlated noise model. In: Proceedings, Flight Mechanics Symposium, Goddard Space Flight Center, Greenbelt, Maryland, NASA Conference Publication, pp. 71–83 (May 1999)